

Supergrowth and sub-wavelength object imaging

Tathagata Karmakar,^{1,2,3,*} Abhishek Chakraborty,^{1,2,3,†} A. Nick Vamivakas,^{4,5,‡} and Andrew N. Jordan^{3,1,2,§}

¹*Department of Physics and Astronomy, University of Rochester, Rochester, NY 14627, USA*

²*Center for Coherence and Quantum Optics, University of Rochester, Rochester, NY 14627, USA*

³*Institute for Quantum Studies, Chapman University, Orange, CA 92866, USA*

⁴*The Institute of Optics, University of Rochester, Rochester, NY 14627, USA*

⁵*Materials Science, University of Rochester, Rochester, NY 14627, USA*

(Dated: July 10, 2023)

We further develop the concept of supergrowth [Jordan, Quantum Stud.: Math. Found. **7**, 285–292 (2020)], a phenomenon complementary to superoscillation, defined as the local amplitude growth rate of a function being higher than its largest wavenumber. We identify the superoscillating and supergrowing regions of a canonical oscillatory function and find the maximum values of local growth rate and wavenumber. Next, we provide a quantitative comparison of lengths and relevant intensities between the superoscillating and the supergrowing regions of a canonical oscillatory function. Our analysis shows that the supergrowing regions contain intensities that are exponentially larger in terms of the highest local wavenumber compared to the superoscillating regions. Finally, we prescribe methods to reconstruct a sub-wavelength object from the imaging data using both superoscillatory and supergrowing point spread functions. Our investigation provides an experimentally preferable alternative to the superoscillation based superresolution schemes and is relevant to cutting-edge research in far-field sub-wavelength imaging.

I. INTRODUCTION

As we strive to engineer optical systems with better imaging capabilities, much attention has been devoted to surpassing the Rayleigh resolution limit in diffraction limited optical devices [1, 2]. To achieve superresolution, methods such as evanescent field based techniques [3, 4] and negative refractive index materials [5] have been proposed. To that end, the efficacy of superoscillatory spot generation for label free far-field based superresolution imaging is well established. Superoscillation (SO) refers to the phenomena of local oscillation frequency of a function being faster than its fastest Fourier component [6–11]. Thus, in optical systems, superoscillation can be utilized to generate sub-wavelength hot-spots and thus beat the Rayleigh resolution limit [12–14]. Sub-wavelength spots have been realized at the focal plane of a microscope objective using optical eigenmode approach implemented with a spatial light modulator [15]. Also, superoscillatory spot properties of radially polarized Laguerre-Gaussian beams in a confocal laser scanning microscopy setup have been studied [16, 17]. Optimization of superoscillatory lenses for sub-diffraction limit optical needle generation has been investigated as well [18].

In principle, it is possible to design arbitrarily small superoscillatory optical spots. However, superoscillation is necessarily accompanied by enhanced side lobes. This leads to poor quality in imaging and unrealistic constraints on the dynamic ranges of the detectors. Several recent ventures try to address this problem through

numerical or design based approaches. Simulations for simultaneous optimization of superoscillatory spot size and their relative intensities compared to the side lobes have been performed [19]. Elimination of sidelobes along a particular dimension by introducing moonlike apertures has been demonstrated [20].

In this work, we show how the problem of enhanced sidelobes can be circumnavigated by utilizing supergrowing functions, a concept proposed by Jordan [21]. The phenomenon of supergrowth (SG) is analogous to superoscillation. While superoscillation pertains to the local oscillation rate of a function, supergrowth occurs when the local growth rate of the amplitude is higher than the highest wave number in the Fourier space of a bandlimited function. A large local growth rate enables enhanced spatial resolution. The idea is analogous to evanescent wave imaging microscopes, but is applicable in the far-field. In our analysis, we consider a canonical single-parameter bandlimited oscillatory function and locate its SO and SG regions. In addition to the entire SO and SG areas, we identify the near maxima regions for both phenomena. We provide analytical estimates for the intensities in these regions and find that the amount of light in the SG areas is exponentially higher compared to the regions associated with SO. Finally, we present two parallel schemes to reconstruct an incoherently illuminated sub-wavelength object with SO and SG point spread functions (PSF). We numerically compare our approaches to object reconstruction using a bandlimited *sinc* PSF. As expected, superresolved object reconstruction is achieved in the former two cases.

The past two decades have witnessed considerable progress in the superoscillation related research. The far-field nature of superoscillatory fields have been shown by proving that subwavelength structures generated by a diffraction grating can survive farther than the evanes-

* tkarmaka@ur.rochester.edu

† achakra9@ur.rochester.edu

‡ nick.vamivakas@rochester.edu

§ jordan@chapman.edu

cent waves [22]. This investigation has inspired further studies into Schrödinger equation based evolution of superoscillatory waves [23–25]. The correspondence between superoscillations and weak values [26, 27] is well known. On a related note, super-phenomena in arbitrary quantum observables [28] have been proposed. Towards the more implementational side, numerical optimization of the energy ratio between superoscillatory region and total signal has been studied [29]. Also new methods for generating superoscillatory functions have been proposed [30–32]. In comparison supergrowth is a very recent concept. Jordan [21] showed that it is possible to access superresolving features using supergrowth. Spherical Bessel function based method for systemic generation of SO/SG functions and general approximation scheme using bandlimited functions have been prescribed [33]. Our analysis draws inspiration from these works and solidifies the benefits of implementing supergrowth based superresolution imaging in practice.

This article is organized as follows. In Sec. II, we briefly describe the phenomena of SO and SG using a canonical oscillatory function. Sec. II A compares the length of SO and SG regions for the chosen function and Sec. II B compares their intensities. In Sec. III, we present the schemes to reconstruct a sub-wavelength object using both superoscillatory and supergrowing spots. In Sec. IV we discuss the implications of our findings. We conclude in Sec. V.

II. PROPERTIES OF SO/SG FUNCTIONS

For our analysis, we consider the function [22]

$$f(x) = (\cos x + ia \sin x)^N, \quad (1)$$

parameterized by a positive real number a , which sets its SO and SG properties, and a natural number N , which gives an upper bound to the Fourier wavenumber $k_{\max} = N$ for the function. This corresponds to a shortest wavelength of oscillation of $\lambda_{\min} = 2\pi/N$. In the following sections we characterize the SO and SG regions of $f(x)$ and look at the intensities within.

A. SO/SG regions

For any complex valued function $f(x)$, the local wavenumber is defined as $k(x) = \text{Im } \partial_x \log f(x)$, and the local growth rate is $\kappa(x) = \text{Re } \partial_x \log f(x)$. If $f(x)$ is bandlimited with highest wavenumber k_{\max} , the function is said to be superoscillating (supergrowing) at x if $|k(x)| > k_{\max}$ ($|\kappa(x)| > k_{\max}$).

For $f(x)$ in Eq. (1), local wavenumber and growth rate take the form [21]

$$k(x) = N \frac{a}{\cos^2 x + a^2 \sin^2 x}, \quad (2)$$

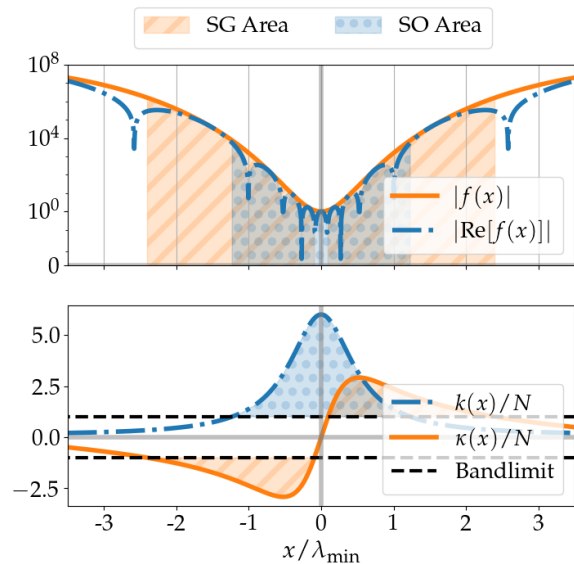


Figure 1. The solid orange (blue dot-dashed) curve in the upper panel shows the magnitude (real part) of the function defined in Eq. (1) in log scale for $a = 6$ and $N = 10$. The vertical grid in the top panel has a spacing equal to the smallest wavelength allowed by the bandlimit. Clearly near $x = 0$ the function oscillates on a scale smaller than the smallest wavelength possible. This is also apparent from the bottom panel where the local rates of oscillation from Eq. (2) (blue dot-dashed line) and growth from Eq. (3) (solid orange line) and are shown as functions of position. The black dashed lines indicate the bandlimit. In both panels, the shaded regions indicate where the function is superoscillating (blue dots) and supergrowing (orange hatching).

and

$$\kappa(x) = N \frac{(a^2 - 1) \sin x \cos x}{\cos^2 x + a^2 \sin^2 x}. \quad (3)$$

For $\sqrt{2} - 1 < a < \sqrt{2} + 1$, this function shows SO, but there is no SG. For $a > \sqrt{2} + 1$, the function displays both SO and SG behavior. We will show in Sec. II B that larger values of a show more SG but less SO, so we will consider only such cases.

Fig. 1 shows the behavior of the function in Eq. (1) (top panel) and the local rates of oscillation and growth in Eqs. (2) and (3) (bottom panel) for $a = 6$ and $N = 10$. The function is superoscillating ($k(x) \geq N$) in $x \in [\arctan(1/\sqrt{a}), \arctan(-1/\sqrt{a})]$, shaded orange in Fig. 1 (bottom panel). The largest local wavenumber is $k(x = 0) = aN$, and it is clear (from top panel) that near origin the function oscillates on a scale shorter than the shortest wavelength.

The function shows SG behavior ($\kappa(x) \geq N$) in $x \in [\arctan y_l, \arctan y_h]$, with

$$y_l = \frac{1}{2} \left(1 - \frac{1}{a^2} - \sqrt{\left(1 - \frac{1}{a^2}\right)^2 - \frac{4}{a^2}} \right), \quad (4)$$

$$y_h = \frac{1}{2} \left(1 - \frac{1}{a^2} + \sqrt{\left(1 - \frac{1}{a^2}\right)^2 - \frac{4}{a^2}} \right).$$

The largest growth rate occurs when $x = \pm x_{sg} = \pm \arctan(a^{-1})$, giving a maximum growth rate of

$$\kappa_{\max} = \pm \frac{N}{2}(a - a^{-1}). \quad (5)$$

For large values of a , this approaches $\pm Na/2$ rapidly.

B. Intensity comparison

In imaging applications, SO/SG spots with higher intensities are ideal since that makes superresolution imaging less susceptible to the influence from sidelobes. In this section, we quantify the amount of light in $f(x)$ in regions showing SO/SG behaviors. For simplicity, we consider the function $f(x)$ to be the intensity point spread function of an incoherent imaging device [34]. The total intensity within a single period of $f(x)$ can be defined as

$$I_0 = \int_{-\pi}^{\pi} dx |f(x)|^2. \quad (6)$$

For large a and N , the total intensity can be approximated as (see Appendix. A)

$$I_0 \approx 2\pi \frac{(2N)!}{(N!)^2} \left(\frac{a}{2}\right)^{2N}. \quad (7)$$

We can further simplify the expression above using Stirling's approximation for factorials

$$I_0 \approx 2\sqrt{\frac{\pi}{N}} a^{2N}. \quad (8)$$

We see indeed that I_0 increases exponentially in N . From Fig. 1, it is clear that the most of this light is available away from the origin. This is a manifestation of pronounced side-lobes around a superoscillatory spot. However, as the subsequent analysis will reveal, SG based imaging can be highly advantageous in this respect.

We see at the superoscillatory region $x = 0$, while the region of superoscillation (where $k > N$) goes from $x \in [-\arctan \frac{1}{\sqrt{a}}, \arctan \frac{1}{\sqrt{a}}]$, the useful range is more restrictive. This is where the oscillations are at their fastest, and the amplitude of oscillations is approximately constant. Noting that $\ln f \approx iaNx + \frac{1}{2}N(a^2 - 1)x^2$, near $x = 0$, we get a more restrictive range $x \in [-1/\sqrt{N(a^2 - 1)}, 1/\sqrt{N(a^2 - 1)}]$. We can find the amount of power in the range by integrating $|f|^2$ over this restrictive interval to find (Appendix. A),

$$I_{\text{SO,R}} \approx \frac{2e^{1/4}}{\sqrt{N(a^2 - 1)}}. \quad (9)$$

We note that the intensity in this region is exponentially suppressed compared to the total intensity in Eqs. (7),(8).

Taking a more relaxed view and using the whole region of superoscillations (even if it becomes impractical to use), we find that integrating over the range $[-\arctan \frac{1}{\sqrt{a}}, \arctan \frac{1}{\sqrt{a}}]$ gives an intensity of

$$I_{\text{SO}} \approx \frac{2a^{N-1/2}}{2N+1}, \quad (10)$$

exponentially smaller than Eq. (8) by a^N .

Let us now consider the SG region characterized by Eq. (4). We find, for $a \gg 1$, κ has the expansion around x_{sg} of $\kappa \approx (aN/2)(1 - (a^2/2)(x - x_{sg})^2)$ to quadratic order. Consequently, we get considerable supergrowth of approximately exponential form in the region $x \in [x_{sg} - 1/a, x_{sg} + 1/a]$. Despite the fact that the phase of f oscillates several times in this region, it is of no concern to us, since we are using only the magnitude (intensity) for the imaging.

Even better exponential fits can be obtained by reducing the range by (say) a factor of 2, but at the cost of reducing the amount of light that is used. The intensity in this reduced region is

$$I_{\text{SG,R}} \approx \frac{1}{a} \left(1 - \frac{1}{a^2}\right)^{N-1} \left(\sum_{m=0}^N \binom{N}{m} \frac{2^{2m+1}}{2m+1} - \frac{5^N}{a^2} \right), \quad (11)$$

which to order $\frac{1}{a}$ is,

$$I_{\text{SG,R}} \approx \sum_{m=0}^N \binom{N}{m} \frac{2^{2m+1}}{2m+1} \frac{1}{a}. \quad (12)$$

It is interesting to note that the intensities in restricted regions Eqs. (9) and (12) both have $1/a$ dependence, instead of the exponential dependence of total intensities in Eqs. (7) and (10). This is due to the shrinking of the restricted regions as a is increased. The coefficient of $1/a$ in the Eq. (12) is much larger than the corresponding coefficient in Eq. (9). Therefore, the near maxima SG region contains more intensity compared to the near maxima SO region. The intensity in the total SG region ($\kappa > 1$ and specified by Eq. (4)) can be approximated as

$$I_{\text{SG}} \approx \frac{\pi}{4} \left(\frac{1}{\sqrt{2}}a\right)^{2N}, \quad (13)$$

We see that the intensity of the SG region is exponentially higher than that of the SO region by a^N , but exponentially smaller than Eq. (8) by $(1/2)^N$. Additionally, the great advantage is that we can profitably use the entire SG range, but only a small fraction of the SO range. This is because the amplitude varies too much once x leaves the more restricted range, as well as the fact that lower values of k become mixed in with the high values (even if still above N). The SG region has none of those drawbacks.

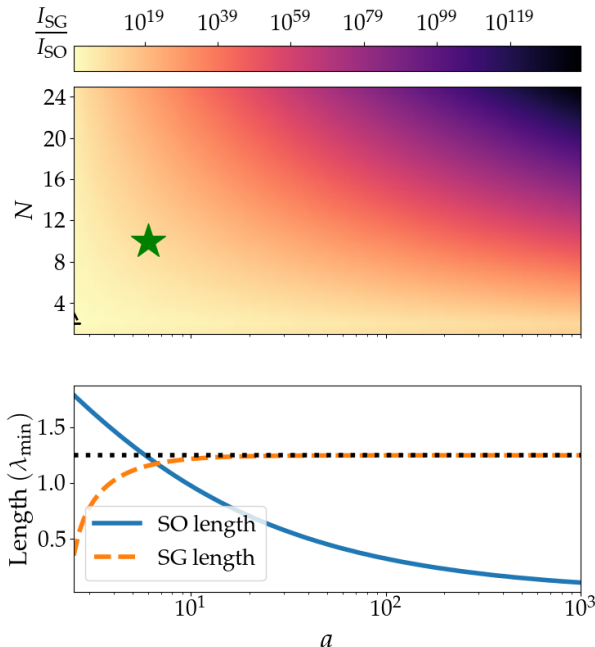


Figure 2. (Top) Ratio of intensities of total SG and SO regions for different values of a and N . With the increase of either a or N , the intensity within the SG region becomes increasingly higher. The dashed black line on the bottom left corner shows the parameter values with equal SO and SG intensities. The green asterisk identifies the region of parameters chosen for object reconstruction scheme presented in Sec. III. (Bottom) Comparison of the lengths of SO and SG regions as a function of a . While the SO region shrinks with the amount of superoscillation (i.e. a), the SG length approaches $1.25\lambda_{\min}$. Note that the full range is N independent.

In Fig. 2, we show quantitative comparisons of SO and SG properties of our chosen function for different values of the parameters a and N . We see that SG intensity dominates SO intensity for most of the parameter range, except for a very small region in the bottom left of the plot. This signifies that for supergrowth imaging can provide a sufficient intensity to obtain bright images, overcoming signal-to-noise ratio issues of superoscillation. We also can compare the lengths of the SO and SG regions with varying a in the bottom panel of Fig. 2. Both of these lengths are independent of N . For large values of a , the length of the SO region $\propto 2a^{-1/2}$ and approaches 0 asymptotically. However, the length of the SG region $\propto \pi/4 - 2a^{-2}$ and rapidly approaches $\pi/4 = 1.25\lambda_{\min}$ asymptotically for large a , which can also be seen in the bottom panel of Fig. 1.

III. SUPERRESOLUTION IMAGING AND OBJECT RECONSTRUCTION

In this section, we present schemes for the detection of sub-wavelength features using SO and SG spots in a diffraction limited optical system. For a simple one-dimensional model of incoherent imaging, we define the function $O(x)$ for the object intensity, and $S(u)$ for the image intensity. They are related via the intensity PSF of the imaging system, $\chi(x)$, which indicates the image created from a point source. Imaging theory dictates

$$S(u) = \int dx O(x) \chi(u-x), \quad (14)$$

so the image created is a convolution of the object with the PSF [1, 35].

We consider the problem of reconstructing $O(x)$ from experimental imaging data $S(u)$ [36]. Now, the Fourier transforms¹ of the above functions are related by

$$\tilde{S}(k) = \tilde{O}(k) \tilde{\chi}(k). \quad (15)$$

If the imaging system is illuminated by light of wavelength $\lambda_0 = 2\pi/k_0$ and has an exit pupil numerical aperture of NA, the PSF and therefore $\tilde{S}(k)$ in Eq. (15) is bandlimited by $k_0\text{NA}$. Inverting the above equation $\tilde{O}(k) = \tilde{S}(k)/\tilde{\chi}(k)$ leads to a loss of information of the higher spatial frequency components and places a constraint on our ability to resolve features smaller than λ_0 .

However, in the following investigation we show how isolating the SO/SG region of the function in Eq. (1) and using that as the PSF can help us resolve sub-wavelength features. This could be done in a confocal imaging setup, where the object is illuminated by a SO/SG optical field spot. As we will see, the nature of SO/SG field spot dictates the near origin features of the image, thereby providing an access to the subwavelength features in the object. In a confocal setup with one objective, the objective NA and wavelength will determine the extent of the spatial filter function that results from the aperture in front of the detector. A pinhole with a deeply subwavelength diameter will still map to a diameter of $\sim \frac{\lambda}{\text{NA}}$ on the object. NA mismatch between illumination and collection is one way to allow for narrow filter functions with respect to SO/SG regions.

In the following analysis, we assume the object has an extent $x \in [-l/2, l/2]$ with $l < \lambda_0$. We can also scan an extended object gradually by filtering length l at a time. For further simplicity, we assume $\text{NA} = 1$ and the object is symmetric (i.e., $O(x) = O(-x)$). Also, in the sample cases we consider, the amplitude PSFs are bandlimited by N . The subsequent analysis separately shows how

¹ Here adopt the convention that the Fourier transform of a function $g(x)$ is $\tilde{g}(k) = \int_{-\infty}^{\infty} \frac{dx}{\sqrt{2\pi}} e^{-ikx} g(x)$, such that the inverse transform is $g(x) = \int_{-k_{\max}}^{k_{\max}} \frac{dk}{\sqrt{2\pi}} e^{ikx} \tilde{g}(k)$.

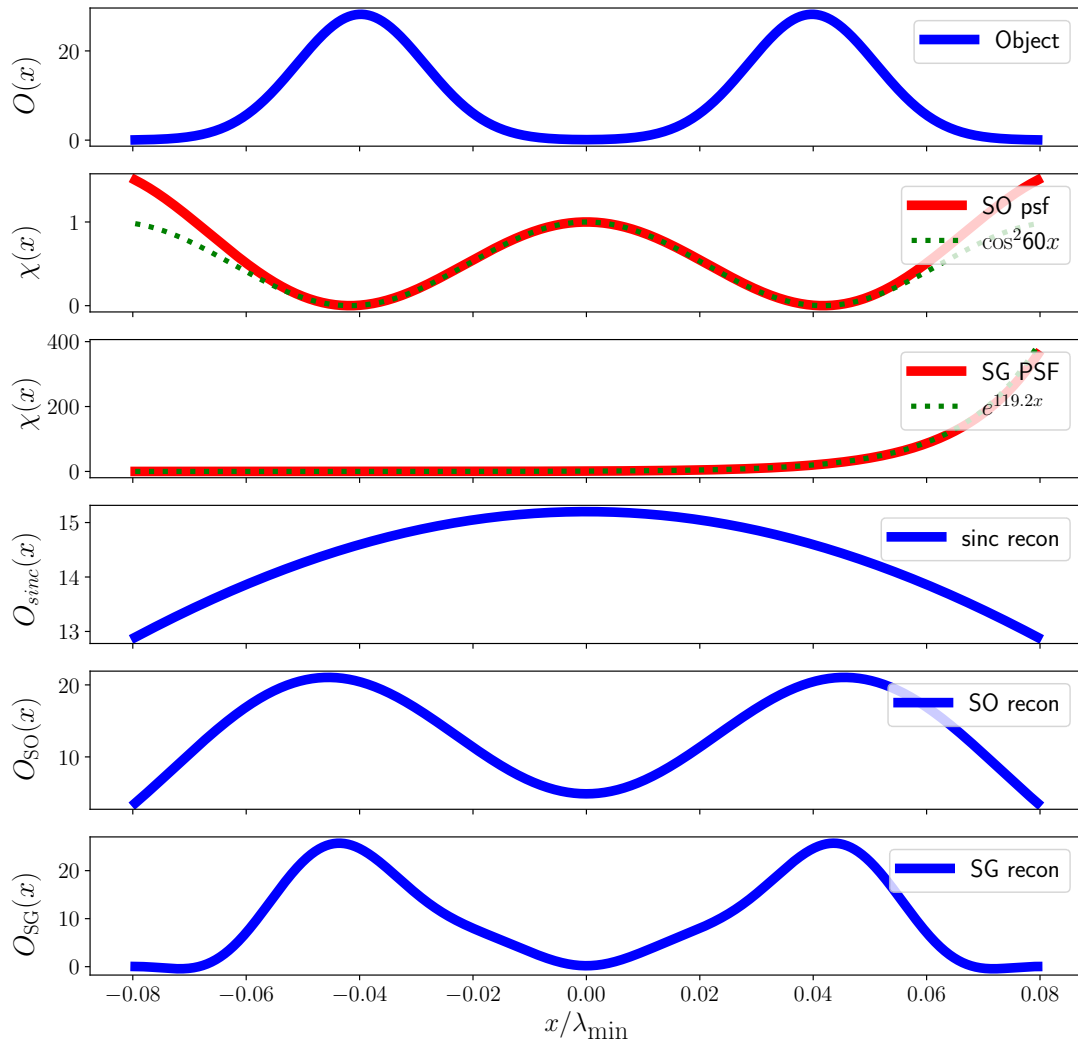


Figure 3. Reconstruction of two sub-wavelength peaks using the methods in Sec. III. The first panel shows the object, which we assume to be two Gaussian peaks separated by a distance of $\sim 0.08\lambda_{\min}$. Throughout the simulations, we assume $N = 10$. The second panel shows the PSF $(\text{Ref}(x))^2$ for $a = 6$ (solid red) and its approximation (green dashed) $\cos^2 60x$ near the origin. The third panel shows the PSF $|f(x)|^2$ (solid red) and its approximation (green dashed) $e^{119.2x}$ centered at $x = x_{sg}$ for $a = 12$. The fourth panel shows object reconstruction with a bandlimited *sinc* PSF using Eq. (15). The fourth and fifth panels show the results from reconstruction using the methods laid out in Secs. III A and III B respectively. We see the superior sub-wavelength feature detection ability of our reconstruction scheme.

SO or SG based imaging can help us reconstruct $O(x)$. We assume, for SO based imaging, the intensity PSF is $(\text{Ref}(x))^2$ while for SG based imaging the relevant PSF is $|f(x)|^2$.

A. Object reconstruction with SO spots

We consider the real part of Eq. (1) as the PSF superoscillating at origin with local rate $k = aN \gg N$. Thus near the origin, for a length larger than the object length l , $\chi(u - x) \sim \cos^2 k(u - x)$ is a good approximation for

the PSF and Eq. (14) can be written as

$$\begin{aligned} S_k(u) &= \int_{-l/2}^{l/2} dx O(x) \cos^2 k(u - x) \\ &= C + \sqrt{\frac{\pi}{2}} \tilde{O}(2k) \cos 2ku, \end{aligned} \quad (16)$$

where for symmetrical objects $\tilde{O}(2k) = \tilde{O}(-2k)$ and C is a constant. The subscript k on S expresses the fact that the observed image intensity depends the chosen PSF. We can invert Eq. (16) or measure the image intensity peak reduction to calculate $\tilde{O}(2k)$. Thus, Eq. (16) provides a prescription for the direct measurement of the high spatial frequency Fourier coefficients of the object.

We can perform a series of measurements with different values of k , i.e. a series of different PSFs, to map out the Fourier transform of the object. If k_{SO} denotes the highest value of the local wavenumber in experiment, the reconstructed object is

$$O_{\text{SO}}(x) = \int_{-2k_{\text{SO}}}^{2k_{\text{SO}}} \frac{dk}{\sqrt{2\pi}} e^{ikx} \tilde{O}(k). \quad (17)$$

B. Object reconstruction with SG spots

In this case, we consider the function in Eq. (1) shifted by x_{sg} such that near origin the PSF can be approximated as $\chi(u-x) \sim e^{\kappa(u-x)}$, where $\kappa = N(a-1/a) \gg N$. Then, we have,

$$S_{\kappa}(u) = \int_{-l/2}^{l/2} dx O(x) e^{\kappa(u-x)}. \quad (18)$$

Assuming a Fourier expansion of $O(x)$ in $x \in [-l/2, l/2]$,

$$O(x) = c_0 + \sum_{n=1}^{\infty} c_n \cos\left(\frac{2\pi nx}{l}\right), \quad (19)$$

Eq. (18) transforms at $u = 0$ to

$$S_{\kappa}(0) = 2 \sinh\left(\frac{\kappa l}{2}\right) \left[\frac{c_0}{\kappa} + \sum_{n=1}^{\infty} (-1)^n c_n \frac{\kappa}{\kappa^2 + \left(\frac{2\pi nx}{l}\right)^2} \right]. \quad (20)$$

Note as n increases, the contributions from higher order terms decrease. In practice the sum on the right hand side will be a good estimate for the left hand side if we consider terms till $n^* = \kappa l$. Again we consider a series of different SG PSFs to measure the left hand side of Eq. (20) as a function of κ . We can then solve for the coefficients numerically to reconstruct the object $O_{\text{SG}}(x)$.

An alternative approach would be to approximate the image intensity in Eq. (18) as a Laplace transform of the object. By performing intensity measurements for different supergrowing PSFs, we gain access to the Laplace transform at different values of κ . The object then can be reconstructed by performing a numerical inverse Laplace transform [37].

One drawback of these schemes is the need to perform imaging using multiple PSFs. In practice, we can limit our experiment to a few different PSFs and use interpolation to approximate \tilde{O} for the intermediate values.

Interestingly, the SO based reconstruction relies on intensity in a small region near origin. Therefore, the method's effectiveness heavily depends on the detector's ability to register small changes in the intensity. On the other hand, the SG based approach does not have this limitation because we only look at the image intensity at a particular point. In experiments, of course, both of these methods will be limited by noise. Having more intensity, SG gives much better SNR.

We show the effectiveness of the schemes in Fig. 3. The top panel shows a sub-wavelength object which is reconstructed using a bandlimited *sinc* function and inverting Eq. (15), and also using SO/SG based schemes described in this section. The second and third panel compare the PSFs for SO and SG imaging for highest values of a (6 and 12 respectively) with their approximation. As we have already seen in Fig. 2, the length of the SO region shrinks with increasing a . This restricts the values of a we can use in practice for SO based reconstruction, while the SG based approach does not have this limitation. In the next panel we immediately see that the cardinal sine function is unable to resolve the two peaks in the reconstructed object as expected. However, as the last two panels show, both the SO and SG PSFs are able to reconstruct the peaks. In the SO based approach, the results of reconstruction are limited by our ability to generate long superoscillatory features for higher values of a . Whereas, in SG based approach, the numerical accuracy in determining the coefficients c_n in Eq. (19) limits the reconstruction. These shortcomings in both cases lead to slightly shifted estimation of the peaks.

IV. DISCUSSION

It was previously shown [21] that the function in Eq. (1) is capable of superresolution imaging using the superoscillation and supergrowth using the function over a full period. For the case of two nearby point sources, putting the point sources in the ‘‘sweet spot’’ of the SO or SG region (maximum $k(x)$ or $\kappa(x)$ respectively) can give superresolution of the two sources. However, due to the nature of the function, any apparatus aiming to use this method would require extremely high dynamic range, both on the illumination and detection side, which limits its utility. We overcome this limitation on the detection side by applying spatial filtering of sweet spot and scanning the image. While both behaviors can resolve features better than the Fourier bound, the SG phenomena benefits from exponentially higher intensity of the illumination point spread function, whereas using SO behavior would require incredibly sensitive detectors due to the exponentially suppressed amplitude. There is also the concern of hitting the diffraction limit for the SO PSF, due to the shrinking length of the region as the parameter a is increased, which is not an issue for the SG case. This demonstrates the superiority of SG spots as a means to achieve superresolution.

V. CONCLUSIONS AND OUTLOOK

We describe supergrowth as a concept analogous to superoscillations, except we evaluate the local growth rate instead of the local wave number of a function. We characterize the supergrowing and superoscillating regions of a canonical oscillatory function as well as provide an-

alytical approximations for the energy inside total supergrowing, total superoscillating, near maxima supergrowing and near maxima superoscillating regions. Our analysis reveals that the supergrowing regions can contain intensity that is exponentially larger in terms of the highest local wavenumber compared to that of the superoscillating regions. These results indicate that superresolution imaging using supergrowing spots could be more advantageous compared to superoscillation based superresolution imaging. Finally, we numerically show that the SO and SG based superresolution imaging is able to reconstruct objects beyond the diffraction limit, thereby demonstrating the efficacy of our schemes.

These findings highlight supergrowth as a potentially superior far-field superresolution scheme. Physically, superoscillation corresponds to rapidly oscillating regions with small amplitude. However, supergrowth, due to high growth rate, connects the smaller amplitude regions with higher amplitude ones. Therefore, it is not surprising that supergrowing regions can contain significantly more light while also giving enhanced resolution. The analytical approximations for intensities characterize the parametric dependence of the light within different regions. These expressions can be useful for designing optimized superoscillatory or supergrowing lenses. Furthermore, the object reconstruction schemes provide the framework for experimental implementation of supergrowth and superoscillation based superresolution imaging.

Our results offer a variety of avenues for potential future investigations. The analysis presented here is restricted to a simple 1-d oscillatory function. Performing similar calculations for more general and higher dimensional functions could have greater significance for experimental implementation of supergrowth imaging. On that note, the natural next step is to investigate ways to generate optimized supergrowing spots. Another relevant problem is to explore whether simultaneous occurrence of superoscillations and supergrowth could be leveraged for better resolution with suppressed side lobe intensity. Apart from the prospective theoretical ventures, a lab realization of supergrowth based superresolution imaging is an imminent experimental challenge. Therefore, our analysis serves as the groundwork for a novel superresolution and object reconstruction scheme with a multitude of scopes for further prospects.

ACKNOWLEDGEMENT

We thank Sethuraj Karimparambil Raju, Sultan Abdul Wadood, Anurag Sahay for providing insight throughout the project. This work has been supported by the AFOSR grant #FA9550-21-1-0322 and the Bill Hannon Foundation.

Appendix A: Intensity calculation

The total intensity (6) can be written as

$$I_0 = 2 \int_{-\frac{\pi}{2}}^{\frac{\pi}{2}} (\cos^2 x + a^2 \sin^2 x)^N dx \quad (\text{A1})$$

A change of variables $y = \tan x$ leads to

$$I_0 = 2 \int_{-\infty}^{\infty} \frac{(1 + a^2 y^2)^N}{(1 + y^2)^{N+1}} dy \quad (\text{A2})$$

Performing a binomial expansion of the numerator and also noting that the integrand is an even function, we can write

$$I_0 = 4 \sum_{m=0}^N \binom{N}{m} \int_0^{\infty} \frac{a^{2m} y^{2m}}{(1 + y^2)^{N+1}} dy. \quad (\text{A3})$$

Adopting another change of variables $y^2 = \frac{z}{1-z}$, the integral $\int_0^{\infty} \frac{y^{2m}}{(1+y^2)^{N+1}} dy$ can be evaluated in terms of Beta functions to be $\frac{1}{2} B(m + \frac{1}{2}, N - m + \frac{1}{2})$. Therefore, using the relationship between Beta and Gamma functions,

$$I_0 = 2 \sum_{m=0}^N \binom{N}{m} \frac{\Gamma(m + \frac{1}{2}) \Gamma(N - m + \frac{1}{2})}{\Gamma(N + 1)} a^{2m}. \quad (\text{A4})$$

For large a and N , we only consider the highest order term in a i.e. a^{2N} . Thus the approximate intensity is

$$I_0 \approx 2\pi \frac{(2N)!}{(N!)^2} \left(\frac{a}{2}\right)^{2N}. \quad (\text{A5})$$

Near the fastest oscillation region $x \in [-(N(a^2 - 1))^{-1/2}, (N(a^2 - 1))^{-1/2}]$, the intensity is

$$I_{\text{SO,R}} = 2 \int_0^{\frac{1}{\sqrt{N(a^2-1)}}} (\cos^2 x + a^2 \sin^2 x)^N dx. \quad (\text{A6})$$

This can be approximated as

$$I_{\text{SO,R}} \approx 2 \int_0^{\frac{1}{\sqrt{N(a^2-1)}}} \exp\{N(a^2 - 1)x^2\} dx. \quad (\text{A7})$$

Now for large a and N , $\frac{1}{\sqrt{N(a^2-1)}} \ll 1$. Using the approximate mean value theorem for integrals, the integration leads to

$$I_{\text{SO,R}} \approx \frac{2e^{1/4}}{\sqrt{N(a^2-1)}}. \quad (\text{A8})$$

The function behaves like $\sim e^{iaN}$ in this restricted region. If we only consider the real part of $f(x)$, i.e. if our PSF is $(\text{Re}f(x))^2$, then the corresponding intensity is almost half of Eq. (A8). Thus, the intensity pertaining to the real part can be approximated as

$$I_{\text{SO,R}}^{\text{Re}} \approx \frac{e^{1/4}}{\sqrt{N(a^2-1)}}. \quad (\text{A9})$$

Next, we look at the total intensity in the superoscillatory spot $x \in [-\arctan \frac{1}{\sqrt{a}}, \arctan \frac{1}{\sqrt{a}}]$, i.e.,

$$I_{\text{SO}} = 2 \int_0^{\tan^{-1} \frac{1}{\sqrt{a}}} (\cos^2 x + a^2 \sin^2 x)^N dx. \quad (\text{A10})$$

Assuming $y = \tan x$, the above integral can be transformed as

$$I_{\text{SO}} = 2 \int_0^{1/\sqrt{a}} \frac{(1 + a^2 y^2)^N}{(1 + y^2)^{N+1}} dy, \quad (\text{A11})$$

with $y \ll 1$ for large a . Using binomial expansion, we can write

$$\begin{aligned} I_{\text{SO}} &= 2 \int_0^{1/\sqrt{a}} dy \left[\sum_{m=0}^N \binom{N}{m} a^{2m} y^{2m} \times \right. \\ &\quad \left. \left(1 - (N+1)y^2 + \frac{(N+1)(N+2)}{2!} y^4 + \dots \right) \right] \\ &= 4 \left[\sum_{m=0}^N \binom{N}{m} \left(\frac{a^{m-1/2}}{2m+1} - \frac{(N+1)a^{m-3/2}}{2m+3} + \dots \right) \right]. \end{aligned} \quad (\text{A12})$$

Taking only the highest order term in a , we get

$$I_{\text{SO}} \approx \frac{2a^{N-1/2}}{2N+1}. \quad (\text{A13})$$

If we only consider the real part of $f(x)$, the intensity within is bounded by Eq. (A13). Therefore, $I_{\text{SO}}^{\text{Re}} \leq I_{\text{SO}}$.

Next we calculate the intensities corresponding to the supergrowing regions. From Eq. (3), we can write κ/N in terms of $y = \tan x$

$$\frac{\kappa}{N} = \frac{(a^2 - 1)y}{1 + a^2 y^2}. \quad (\text{A14})$$

The region of supergrowth corresponds to $y_l < y < y_h$, where

$$\begin{aligned} y_l &= \frac{1}{2} \left(1 - \frac{1}{a^2} - \sqrt{\left(1 - \frac{1}{a^2}\right)^2 - \frac{4}{a^2}} \right), \\ y_h &= \frac{1}{2} \left(1 - \frac{1}{a^2} + \sqrt{\left(1 - \frac{1}{a^2}\right)^2 - \frac{4}{a^2}} \right). \end{aligned} \quad (\text{A15})$$

Similarly, the superdecaying region corresponds to $-y_h < y < -y_l$.

Now, we consider the near extrema ($x_{sg} = \arctan \frac{1}{a}$) region for the supergrowth. The point of extrema can be written as $\tan^{-1} \frac{1}{a} = \left(\frac{1}{a} - \frac{1}{3a^3} + \frac{1}{5a^5} - \dots \right)$. Therefore, $x \in [x_{sg} - 1/a, x_{sg} + 1/a]$ corresponds to the total region of $\sim [-\frac{1}{3a^3}, \frac{2}{a} - \frac{1}{3a^3}]$. However, since $\arctan y_l > 0$, the region of interest should instead be $\sim [\arctan y_l, x_{sg} + 1/a]$. Thus,

$$I_{\text{SG,R}} = \int_{\arctan y_l}^{x_{sg} + \frac{1}{a}} (\cos^2 x + a^2 \sin^2 x)^N dx. \quad (\text{A16})$$

With the change in variable $x' = x - x_{sg}$, we can write

$$\begin{aligned} I_{\text{SG,R}} &= \left(\frac{2a^2}{1+a^2} \right)^N \times \\ &\quad \int_{\arctan y_l - \arctan \frac{1}{a}}^{\frac{1}{a}} \left(1 + \rho \sin x' \cos x' + \frac{1}{2} \rho^2 \sin^2 x' \right)^N dx', \end{aligned} \quad (\text{A17})$$

where $\rho = a - \frac{1}{a}$. For large a , the interval could be approximated as $[-\frac{1}{a}, \frac{1}{a}]$, and the integral is approximately

$$I_{\text{SG,R}} \approx \left(\frac{2a^2}{1+a^2} \right)^N \int_{-\frac{1}{a}}^{\frac{1}{a}} \left(1 + \rho x' + \frac{1}{2} \rho^2 x'^2 \right)^N dx'. \quad (\text{A18})$$

Performing the integral leads to

$$\begin{aligned} I_{\text{SG,R}} &\approx \left(\frac{a^2}{1+a^2} \right)^N \times \\ &\quad \sum_{m=0}^N \frac{1}{\rho} \binom{N}{m} \frac{(1 + \rho/a)^{2m+1} - (1 - \rho/a)^{2m+1}}{2m+1}. \end{aligned} \quad (\text{A19})$$

For $a, N \gg 1$, this could be further approximated to

$$I_{\text{SG,R}} \approx \frac{1}{a} \left(1 - \frac{1}{a^2} \right)^{N-1} \left(\sum_{m=0}^N \binom{N}{m} \frac{2^{2m+1}}{2m+1} - \frac{5^N}{a^2} \right). \quad (\text{A20})$$

The intensity first increases, then decreases as a function of a . This is because at the value of the function $f(x)$ increases with a . However, as we keep increasing a , the length of the restricted region gets smaller leading to a decrease in the intensity. The approximate value of a with maximum $I_{\text{SG,R}}$, denoted as a^* , could be calculated by differentiating the above expression. Assuming, $C_N = \sum_{m=0}^N \binom{N}{m} \frac{2^{2m+1}}{2m+1}$, $\gamma_N = 5^N/C_N$ and $\beta_N = \frac{1}{2} (2N - 1 + 3\gamma_N)$, we get

$$a^*(N) \approx \sqrt{\sqrt{\beta_N^2 - \gamma_N} + \beta_N}. \quad (\text{A21})$$

Lastly, we consider the total intensity in the supergrowing region

$$I_{\text{SG}} = \int_{\arctan y_l}^{\arctan y_h} (\cos^2 x + a^2 \sin^2 x)^N dx. \quad (\text{A22})$$

For large a , the upper and lower bounds can be approximated to be 0 and $\pi/4$ respectively. Similar to Eq. (A3) the integration above can be written as

$$I_{\text{SG}} \approx \sum_{m=0}^N \binom{N}{m} \int_0^1 \frac{a^{2m} y^{2m}}{(1+y^2)^{N+1}} dy. \quad (\text{A23})$$

Only limiting to highest order term in a leads to

$$I_{\text{SG}} \approx F_N a^{2N}, \quad (\text{A24})$$

where

$$F_N = \int_0^1 dy \frac{y^{2N}}{(1+y^2)^{N+1}}, \quad (\text{A25})$$

can be evaluated using the recurrence relation

$$F_N = (1 - \frac{1}{2N})F_{N-1} - \frac{1}{2^{N+1}N}, \quad (\text{A26})$$

and $F_0 = \pi/4$. We can find the asymptotic value

of F_N by transforming the integral in Eq. (A25) with $y = \tan \theta$. Then, $F_N = \int_0^{\pi/4} d\theta \sin^{2N} \theta$. The integral can be expressed in terms of incomplete Beta function as $F_N = \frac{1}{2} B_{\frac{1}{2}}(N + \frac{1}{2}, \frac{1}{2})$. As N increases, the integrand approaches zero. We approximate $\sin \theta \approx \frac{1}{\sqrt{2}}$ in the interval $\theta \in [0, \pi/4]$. Thus, $F_N \sim (1/2)^N \frac{\pi}{4}$.

-
- [1] J. W. Goodman, *Introduction to Fourier Optics*, fourth edition ed. (W.H. Freeman, Macmillan Learning, New York, 2017).
- [2] W. Lukosz, *Journal of the Optical Society of America* **56**, 1463 (1966).
- [3] D. W. Pohl, W. Denk, and M. Lanz, *Applied Physics Letters* **44**, 651 (1984).
- [4] H. Yang, N. Moullan, J. Auwerx, and M. A. M. Gijs, *Small* **10**, 1712 (2014).
- [5] J. B. Pendry, *Phys. Rev. Lett.* **85**, 3966 (2000).
- [6] Y. Aharonov, S. Popescu, and D. Rohrlich, Tel-Aviv University Preprint TAUP **1847–90**.
- [7] P. Ferreira and A. Kempf, *IEEE Transactions on Signal Processing* **54**, 3732 (2006).
- [8] A. Kempf, *Journal of Mathematical Physics* **41**, 2360 (2000).
- [9] A. Kempf, *Quantum Studies: Mathematics and Foundations* **5**, 477 (2018).
- [10] E. Tang, L. Garg, and A. Kempf, *Journal of Physics A: Mathematical and Theoretical* **49**, 335202 (2016).
- [11] G. Chen, Z.-Q. Wen, and C.-W. Qiu, *Light: Science & Applications* **8**, 56 (2019).
- [12] M. V. Berry and S. Popescu, *J. Phys. A: Math. Gen.* **39**, 6965 (2006).
- [13] M. Berry, N. Zheludev, Y. Aharonov, F. Colombo, I. Sabadini, D. C. Struppa, J. Tollaksen, E. T. Rogers, F. Qin, M. Hong, *et al.*, *Journal of Optics* **21**, 053002 (2019).
- [14] E. T. F. Rogers and N. I. Zheludev, *Journal of Optics* **15**, 094008 (2013).
- [15] J. Baumgartl, S. Kosmeier, M. Mazilu, E. T. F. Rogers, N. I. Zheludev, and K. Dholakia, *Applied Physics Letters* **98**, 181109 (2011).
- [16] Y. Kozawa and S. Sato, *Optics Express* **23**, 2076 (2015).
- [17] Y. Kozawa, D. Matsunaga, and S. Sato, *Optica* **5**, 86 (2018).
- [18] J. Diao, W. Yuan, Y. Yu, Y. Zhu, and Y. Wu, *Optics Express* **24**, 1924 (2016).
- [19] K. S. Rogers, K. N. Bourdakos, G. H. Yuan, S. Mahajan, and E. T. F. Rogers, *Optics Express* **26**, 8095 (2018).
- [20] Y. Hu, S. Wang, J. Jia, S. Fu, H. Yin, Z. Li, and Z. Chen, *Advanced Photonics* **3**, 045002 (2021).
- [21] A. N. Jordan, *Quantum Studies: Mathematics and Foundations* **7**, 285 (2020).
- [22] M. V. Berry and S. Popescu, *Journal of Physics A: Mathematical and General* **39**, 6965 (2006).
- [23] F. Colombo, J. Gantner, and D. C. Struppa, *Journal of Mathematical Physics* **58**, 092103 (2017).
- [24] Y. Aharonov, F. Colombo, I. Sabadini, D. C. Struppa, and J. Tollaksen, *Annals of Physics* **414**, 168088 (2020).
- [25] M. V. Berry and S. Fishman, *Journal of Physics A: Mathematical and Theoretical* **51**, 025205 (2018).
- [26] M. Nairn, “Superoscillations: Realisation of quantum weak values,” (2021), [arXiv:2109.14404](https://arxiv.org/abs/2109.14404) [quant-ph].
- [27] M. V. Berry and P. Shukla, *Journal of Physics A* **45**, 015301 (2012).
- [28] A. N. Jordan, Y. Aharonov, D. C. Struppa, F. Colombo, I. Sabadini, T. Shushi, J. Tollaksen, J. C. Howell, and A. N. Vamivakas, “Super-phenomena in arbitrary quantum observables,” (2022), [arXiv:2209.05650](https://arxiv.org/abs/2209.05650) [math-ph, physics:quant-ph].
- [29] E. Katzav and M. Schwartz, *IEEE Transactions on Signal Processing* **61**, 3113 (2013).
- [30] Y. Aharonov, F. Colombo, I. Sabadini, D. C. Struppa, and J. Tollaksen, in *Quantum Theory: A Two-Time Success Story*, edited by D. C. Struppa and J. M. Tollaksen (Springer Milan, Milano, 2014) pp. 313–325.
- [31] M. Smith, *Optical Vortices and Coherence in Nano-Optics*, Ph.D. thesis (2019).
- [32] L. Chojnacki and A. Kempf, *Journal of Physics A: Mathematical and Theoretical* **49**, 505203 (2016).
- [33] T. Karmakar and A. N. Jordan, “Beyond superoscillation: General theory of approximation with bandlimited functions,” (2023), [arXiv:2306.03963](https://arxiv.org/abs/2306.03963) [math-ph].
- [34] T. Wilson, *Journal of Microscopy* **244**, 113 (2011).
- [35] M. Born and E. Wolf, *Principles of Optics: Electromagnetic Theory of Propagation, Interference and Diffraction of Light*, 7th ed. (Cambridge University Press, Cambridge ; New York, 1999).
- [36] C. W. Barnes, *J. Opt. Soc. Am.* **56**, 575 (1966).
- [37] A. M. Cohen, *Numerical Methods for Laplace Transform Inversion* (Springer, New York, NY, 2007).